Synthesis and Characterization of Nonlinear Nanopores in Alumina Films

Rashid Zakeri,[†] Clay Watts,[‡] Haibo Wang,[§] and Punit Kohli*[,†]

Departments of Chemistry and Biochemistry, Physics, and Electrical Engineering, Southern Illinois University, Carbondale, Illinois 62901

Received October 31, 2006. Revised Manuscript Received December 20, 2006

Controlled and convenient synthetic approaches for more complex-shaped nanotubes and nanowires of different materials are needed to further advance the field of nanoscience and nanotechnology. In this paper, we report the synthesis and characterization of nonlinear nanopores (such as curved and dendritic nanopores) containing alumina films. We show that control over the orientation of nanopores can be accomplished by controlling the geometric shape of aluminum substrates on which nanoporous alumina is grown. The anodically grown alumina on square and rectangular aluminum substrates showed cracks at the sharp edges of the substrates but no cracks were observed in nanoporous alumina films grown on cylindrical substrates. Our electrostatic calculations suggest that the electric field intensity at sharp edges of the rectangular/square substrates is significantly larger than that at the flat faces of the substrates. This leads to a faster alumina growth rate and hence increased stresses at these edges. We also propose a simple model that predicts the shape and orientation of nonlinear nanopores grown on different geometric shaped substrates. Through the use of proposed nanoporous films as template, one can easily synthesize highly complex-shaped nanotubes and nanowires of different materials.

I. Introduction

Nanoporous membranes have been extensively used for many applications, including biomolecule separations and sensing,[1−6] magnetic storage,[7] solar energy applications,[8] carbon nanotube synthesis,[9,10] and the synthesis of functional multisegment nanorods.[4,11,12] These membranes are usually available in many matrices such as alumina, polycarbonate, and polyester. Alumina nanoporous membranes have some advantages over polymer membranes. The alumina membranes have higher pore density up to $\sim 10^{11}$ pores/cm^2 and narrow pore diameter distribution. They are resistant to organic solvents and can be used at a very high temperature (>1000 °C). They are also easy to produce in the laboratory and have a low processing cost. The diameter and density of pores in the alumina films can be controlled by the appropriate choice of temperature and concentration of electrolyte solution (such as sulfuric acid, phosphoric acid, and oxalic acid) and applied voltage between the aluminum substrate and a cathode.[13,14] Similarly, the length of the nanopores can be easily controlled with anodizing time.[13,14]

Most of the studies to date have been focused on linear nanopores in the alumina membranes synthesized on flat aluminum sheets or foils. The pores are usually grown perpendicular to the surface of the aluminum sheet, and very thick membranes of tens to hundreds of micrometers have been synthesized.[15] Recently, aluminum stripes have been embedded between silicon oxide layers, and the electric field was forced in a direction parallel to the aluminum surface.[16a,16b] This alumina growth resulted in alumina nanopores running parallel to the aluminum surface. Similarly, Y-junction carbon nanotubes,[24] metallic conical nanotubes and nanowires,[16c−e] and tri-, tetra- and higher-ordered branched nanorods[16f] have also recently been prepared.

* Corresponding author. E-mail: pkohli@chem.siu.edu.
[†] Department of Chemistry and Biochemistry, Southern Illinois University.
[‡] Department of Physics, Southern Illinois University.
[§] Department of Electrical Engineering, Southern Illinois University.

(1) (a) Martin, C. R. *Science* **1994**, *266*, 1961−1966. (b) Martin, C. R.; Kohli, P. *Nat. Drug Discovery* **2003**, *2*, 29−27.
(2) (a) Kohli, P.; Harrell, C. C.; Zehui, C.; Gasparac, R.; Tan, W.; Martin, C. R. *Science* **2004**, *305*, 984−986. (b) Lee, S. B.; Mitchell, D. T.; Trofin, L.; Nevanen, T. K.; Soderlund, H.; Martin, C. R. *Science* **2002**, *296*, 2198−2200.
(3) Harrell, C. C.; Kohli, P.; Siwy, Z.; Martin, C. R. *J. Am. Chem. Soc.* **2004**, *126*, 15646−15647.
(4) Nice Warner-Pena, S. R.; Freeman, R. G.; Reiss, B. D.; He, L.; Pena, D. J.; Walton, I. D.; Cromer, R.; Keating, C. D.; Natan, M. J. *Science* **2001**, *294*, 137.
(5) Roa, S. G.; Huang, L.; Setyawan, W.; Hong, S. *Nature* **2003**, *425*, 36.
(6) Chou, S. Y.; Keimel, C.; Gu, J. *Nature* **2002**, *417*, 835.
(7) Metzger, R. M.; Konovalov, V. V.; Sun, M.; Xu. T.; Zangari, G.; Xu, B.; Benahli, M.; Doyle, W. D. *IEEE Trans. Magn.* **2000**, *36*, 30−35.
(8) (a) Karmhag, R.; Tesfamicheal, T.; Wackelgard, E.; Niklasson, G. A.; Nygren, M. *Solar Energy* **2000**, *68*, 329−333. (b) Huang, S.; Efstathiadis, H.; Haldar, P.; Lee, H.-G.; Landi, B.; Raffaelle, R. *Mater. Res. Soc. Symp. Proc.* **2005**, *836*, 49−53.
(9) Che, G.; Lakshmi, B. B.; Fisher, E. R.; Martin, C. R. *Nature* **1998**, *393*, 346.
(10) Miller, S. A.; Young, V. Y.; Martin, C. R. *J. Am. Chem. Soc.* **2001**, *123*, 12335−12342.
(11) Hurst, S. J.; Payne, E. K.; Qin, L.; Mirkin, C. A. *Angew. Chem., Int. Ed.* **2006**, *45*, 2672−2692 and references therein.
(12) Park, S.; Lim, J.-H.; Chung, S.-W.; Mirkin, C. A. *Science* **2004**, *303*, 348−351.
(13) Ono, S.; Saito, M.; Asoh, H. *ATB Metall.* **2003**, *43*, 41−44.
(14) (a) Jessensky, O.; Muller, F.; Gosele, U. *Appl. Phys. Lett.* **1998**, *72*, 1173−1175. (b) Bandyopadhyay, S.; Miller, A. E.; Chang, H. C.; Banerjee, G.; Yuzhakov, V.; Yue, D.-F.; Ricker, R. E.; Jones, S.; Eastman, J. A.; Baugher, E.; Chandrasekhar, M. *Nanotechnology* **1996**, *7*, 360−371. (c) O' Sullivan, J. P.; Wood, G. C. *Proc. R. Soc. London, Ser. A* **1970**, *317*, 511.
(15) Nielsch, K.; Choi, J.; Schwirn, K.; Wehrspohn, R. B.; Gosele, U. *Nano Lett.* **2002**, *2*, 677−680.

10.1021/cm062595o CCC: $37.00
Published on Web 03/24/2007

In this paper, we report the synthesis and characterization of nonlinear pores containing alumina films that can be used as templates[1] for the synthesis of complex shaped nanotubes and nanowires in a large quantity. We demonstrate that the geometric shape of aluminum substrates strongly affects the nanopore characteristics such as orientation, pore density, and merging and curving of pores in the alumina films. We also propose a mechanism that explains the orientation of synthesized nanopores grown on different geometrical aluminum substrates. By using these nanoporous alumina films as templates, it is possible to prepare inexpensive, complex-shaped nanotubes and nanowires in large quantities that are otherwise difficult to synthesize. The use of complex-shaped nanopores would open new and exciting opportunities for potential applications in the fields of nanodevice (such as nanoelectronic and nanofluidic) fabrication, biosensing, bioseparations, and catalysis.

II. Materials and Methods

All the chemicals were purchased from Fisher Scientific and used as received, unless otherwise noted. The aluminum substrates (Alfa Aeser, purity >99.81%) were anodically oxidized using a two-step growth process reported by Masuda and co-workers.[18] Briefly, the aluminum substrates were cut into desired sizes and geometric shapes using an electric saw. The substrates were sanded with 400, 600, and 1500 grit sand papers and washed and sonicated sequentially in soap, water, and ethanol. The annealing of aluminum was carried out at 500 °C for 24 h. Electropolishing of the aluminum was carried out in a solution composed of 95% H_3PO_4 (wt/wt), 5% H_2SO_4 (wt/wt), and 0.2 M CrO_3 at 15 V for 27 min followed by thorough washing in deionized water. The electropolishing of aluminum makes it extremely reflective and smooth (see the Supporting Information, Figure 1S). In the first anodic oxidation step, the alumina nanopores were grown in a 0.4 M oxalic acid solution for ~3−6 h on the electropolished aluminum substrates. The alumina film was then dissolved in a solution of 0.2 M CrO_3 and 0.4 M H_3PO_4 at ~72 °C. This solution etched away only alumina, leaving behind a highly ordered scallop pattern on which ordered nanopores were grown in the second anodic step. The second anodic alumina growth was then performed in 0.4 M oxalic acid for 12−24 h. All experiments were conducted at 60 V at a constant temperature of 0 °C (±0.5 °C).

The characterization of alumina films was carried out using a Hitachi 570 scanning electron microscope (SEM) and H7000 transmission electron microscope (TEM). The samples for SEM analysis were made conductive by coating a thin gold film (5−10 nm) using a Denton III sputter. All the scanning electron micrographs (SEMs) were taken on alumina films without any post-chemical etching.

The template synthesis[1] of silica nanotubes in the nanoporous films was performed using a published procedure.[2b] Briefly, 5 mL of tetraethoxysilane (TEOS) is mixed with 95 mL of ethanol and 1 mL of 1M HCl. This solution was stirred for about 30 min to promote polymerization of silica formation. The alumina films were then soaked in the sol−gel solution for 45 min followed by thorough washing in ethanol and curing of silica at 120 °C for 4 h to complete the polymerization process. The silica nanotubes were then liberated by dissolving away the alumina template by soaking in an aqueous solution of phosphoric acid (5%) overnight.

To gain more knowledge about intensity and orientation of the electric field during alumina growth, we performed electrostatic field calculations by solving poisson's equation using Flex-PDE 5.0.11 software. These calculations gave insight into orientation of the nanopores in the alumina films. The calculations were performed on square- and cylindrical-shaped aluminum substrates. The dimensions of anodes were 20 times smaller than those of cylindrical cathode and a voltage of 60 V was used for all the calculations. To simplify calculations, we neglected the alumina barrier layer at the aluminum/alumina interface. More details on the calculations can be found in the Supporting Information accompanying this manuscript (Figures 4S and 5S).

Before we discuss our results, we present in Table 1 the nomenclature of various substrates used. This table contains the dimensions, geometries, and schematic diagrams of different substrates used in this study.

III. Results and Discussions

IIIA. Nanoporous Alumina Grown on Planar and Rectangular Substrates. A scanning electron micrograph of nanoporous alumina grown on a planar 5×5 cm^2 aluminum plate is shown in Figure 1. The self-organized, well-ordered, and hexagonally packed pores were grown perpendicular to the surface. The monodispersed pores are ~50 nm in diameter, with a pore density of $\sim 1.6 \times 10^{10}$ pores/cm^2. In contrast to anodic alumina grown on a flat aluminum plate, the pores grown on a rectangular cross section rod (dimension: ~300 μm × 450 μm × 3 cm) under the same experimental conditions have some unique characteristics. First, the growth of nanopores is always perpendicular to the Al surface (see four insets in Figure 2A). The pores (60−90 nm in diameter and ~70 μm in length) grown on the flat faces of the aluminum substrate are self-ordered, monodisperse, and parallel to each other. Second, the direction of the growth of alumina on one face of the rectangular substrate is ~90° rotated from the nanopores grown on its adjacent face of the substrate. Third, we found cracks in the alumina films grown on the rectangular substrates. The cracks are shown in Figure 2A by arrows at the four edges of the substrate. These cracks can also be observed under a low-magnification eye piece (×20 magnification) when thick alumina films (>40 μm) were grown. Fourth, the cracks in nanoporous alumina films were not observed on cylindrical aluminum substrates of 450−1000 μm in diameter under the same anodic conditions even when films >50 μm in thickness were grown. Fifth, for films grown on the rectangular or square substrates, the pore density away from and near (or in) the cracks were the same (~7×10^9 pores/cm^2). However, the pore diameter near and

(16) (a) Cojocaru, C. S.; Padovani, J. M.; Wade, T.; Mandoli, C.; Jaskierowicz, G.; Wegrowe, J. E.: Morral, A. F. i.; Pribat, D. *Nano Lett.* **2005**, *5*, 675−680. (b) Chen, Z.; Zhang, H. *J. Electrochem. Soc.* **2005**, *152*, D227−D231. (c) Siwy, Z. S.; Fulinski, A. *Phys. Rev. Lett.* **2002**, *89*, 198103/1−19810.3/4. (d) Siwy, Z. S. *Adv. Funct. Mater.* **2006**, *16*, 735−746. (e) Harrell, C. C.; Ziwy, Z. S.; Martin, C. R. *Small* **2006**, *2*, 194−198. (f) Milliron, D. J.; Hughes, S. M.; Cui, Y.; Manna, L.; Wang, L.-W.; Alivisatos, A. P. *Nature* **2004**, *430*, 190−195.
(17) (A) Rabin, O.; Herz, P. R.; Lin, Y. -M.; Akinwande, A. I.; Cronin, S. B.; Dresselhaus, M. S. *Adv. Funct. Mater.* **2003**, *13*, 631−638. (B) Yan, J.; Rama Rao, G. V.; Berala, M.; Brevnov, D. A.; Jiang, Y.; Xu, H.; Lopez, G. P. Atanassov, P. B. *Adv. Mater.* **2003**, *15*, 2015−2018.
(18) Masuda, H.; Fukuda, K. *Science* **1995**, *268*, 1466.
(19) Feiyue, L.; Zhang, L.; Metzger, R. M. *Chem. Mater.* **1998**, *10*, 2470−2480.
(20) Sulka, G. D.; Stroobants, S.; Moshchalkov, V. V.; Borghs, G.; Celis, J.-P. *J. Electrochem. Soc.* **2004**, *151*, B260−B264.

Table 1. Nomenclature, Details, and Schematic Diagrams of Different Substrates Used in This Study[a]

Nomenclature	Details	Schematic Diagram
Flat/planar	Aluminum substrates whose two dimensions are much larger than the third dimension. For example, flat substrates of 5 cm x 5 cm x 110 μm were used in the present studies.	
Rectangular	Aluminum substrates with rectangular cross-section and whose one dimension is much larger than other two dimensions. Dimensions: 300 μm x 450 μm x 3 cm.	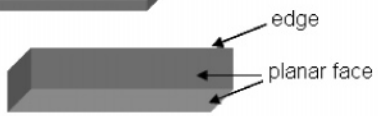
Cylindrical	Aluminum substrates with circular cross-section. Dimensions: diameter ranging between 450 μm and 1000 μm, and length 3 cm.	
Hexagonal	Aluminum substrates with hexagonal cross-section. Dimensions are similar to rectangular and circular substrates.	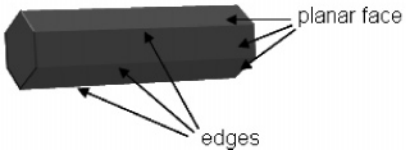

[a] Note that "planar face" is labeled in the rectangular and hexagonal schematic diagrams. "Edges" where two planes intersect are also labled for rectangular and hexagonal substrates.

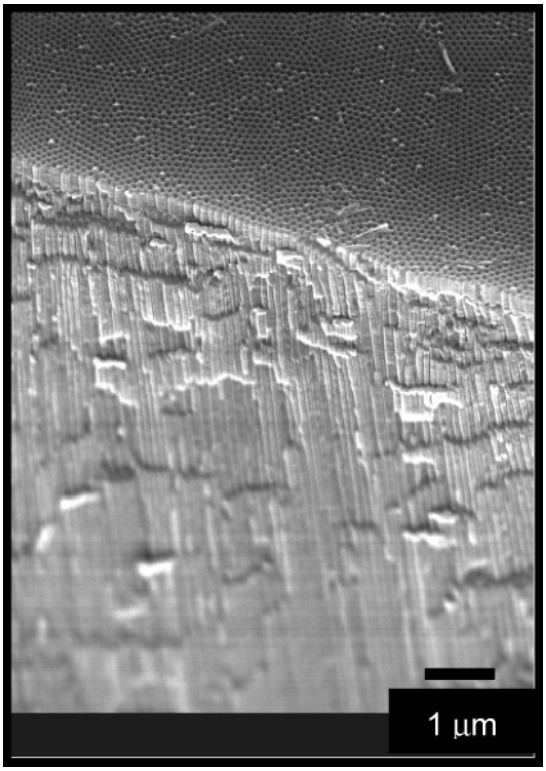

Figure 1. Nanoporous alumina film grown on a flat aluminum foil at 45 V using a two-step method reported by Masuda and co-workers.[18] The pores were self-organized, well-ordered, and hexagonally packed, and the orientation of pores was perpendicular to the surface. The pore diameter was ~50 nm.

away from cracks showed some significant differences. The pore diameter away from the cracks had a relatively narrow distribution (75 ± 10 nm), but pores near/in the cracks showed a wider pore diameter distribution and were not hexagonally packed. Some pores were as big as 120 nm ,-whereas others ~40 nm in diameter were observed in/near the cracks created in the film.

We now discuss the origin of cracks in the anodically oxidized alumina films prepared on rectangular and square aluminum substrates and the lack of cracks on the cylindrical substrates under the same experimental conditions. For self-organized nanoporous alumina membranes, a volume expansion of about 20−60% is reported when aluminum is electrochemically oxidized to alumina.[14,21] The volume expansion during alumina growth generates large compressive stresses in the films. On the planar substrates and planar faces (except at four edges) of rectangular substrates, the compressive stress generated due to volume expansion during alumina growth is uniform on the whole substrate. Because of unrestricted lateral geometry of the planar substrates and the planar faces of rectangular, square and triangular substrates, the oxide films can be expanded in both upward and lateral directions without significant spatial constraints. The stress is, thus, uniformly distributed over the whole of the planar faces except at the sharp edges. On the other hand, the volume expansion at geometrically restricted edges (where two planar faces meet) of the square and rectangular substrates is severely constrained. This results in large compressive stresses at these edges. Further, our electric field calculations suggest that the electric field at the sharp edges (~7.5×10^5 V/m) of the square substrates is about 50% larger than that of planar faces of the substrate (~4×10^5 V/m; Figure 2B). This is clearly seen as four sharp peaks in the electric field intensity plot (Figure 2B). The implication of this enhanced electric field is that the alumina growth is

(21) Li, A. P.; Muller, F.; Birner, A.; Nielsch, K.; Gosele, U. *J. Appl. Phys.* **1998**, *84*, 6023−6026.
(22) Gallas, M. R.; Piermarini, G. J. *J. Am. Ceram. Soc.* **1994**, *77*, 2917−2920.
(23) Callister, W. D. *Materials Science and Engineering an Introduction*, 5th ed.; John Wiley & Sons: New York, 2004.
(24) (a) Li, J.; Papadopoulos, C.; Xu, J. *Nature* **1999**, *402*, 253−254. (b) Meng, G.; Jung, Y. J.; Cao, A.; Vajtai, R.; Ajayan, P. M. *Proc. Natl. Acad. Sci. U.S.A.* **2005**, *102*, 7074−7078.

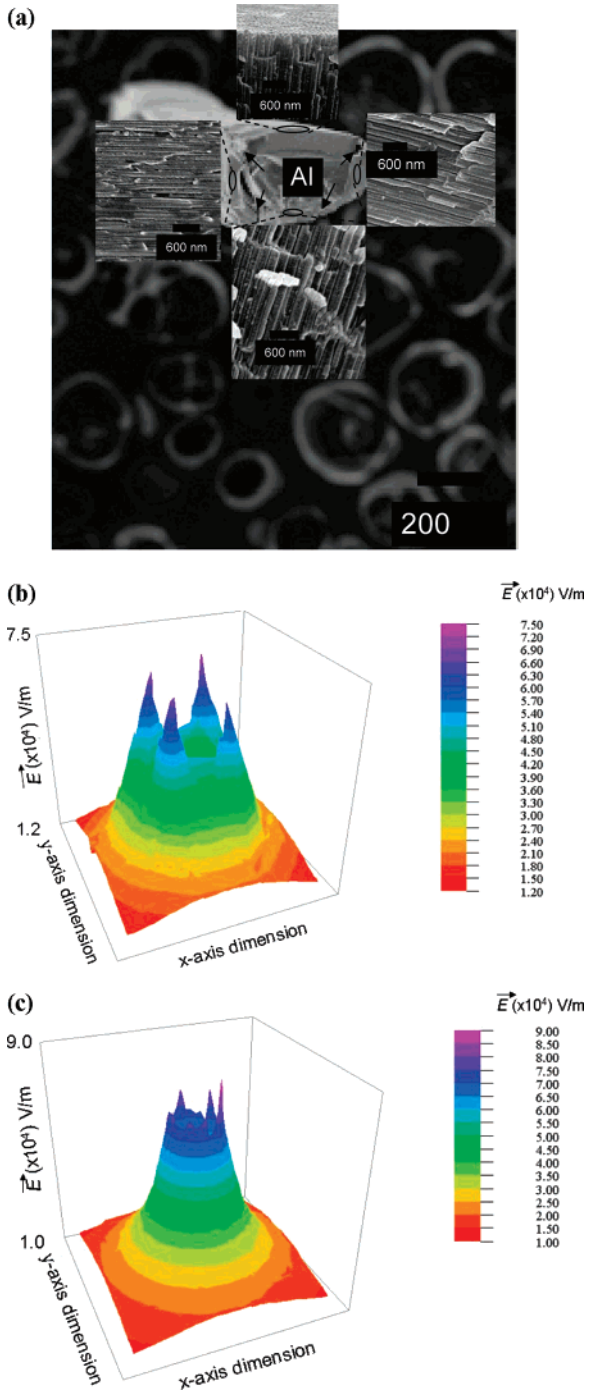

Figure 2. (A) Cross-sectional scanning electron micrograph (SEM) of anodic alumina grown on a rectangular aluminum rod (~300 μm × 450 μm) at 60 V in 0.4 M oxalic acid. "Al" in the middle of this figure denotes an aluminum rod that is partially oxidized to alumina. The electron micrograph was taken after cutting the rod along its cross-section. The growth of Al_2O_3 was always perpendicular to the Al surface (see four inset figures). The growth direction of alumina nanopores on one face of the substrate is 90° rotated from the nanopores grown on its adjacent face of the substrate. The arrows in this figure represent cracks formed after anodization. (B) Electric field plots for a square aluminum substrate. The electric field intensity is depicted along the *z*-axis, whereas the *x*- and *y*-axes represent the distance between cathode and anode. For example, $x = 0$ and $y = 0$ represent the center of the anode. Different colors in the figure show the intensity of the electric field at those points. For example, purple and red circles denote an isoelectric field potential of ~75 and ~12 kV/m, respectively. Note that there are four sharp spikes at four edges of the square substrate, which indicates a much larger calculated electric field strength at the edges than those calculated at the flat faces of the substrate. (C) Corresponding electric field intensity plot for a cylindrical substrate. The electric field intensity plot indicates a much smoother electric field at the cylindrical surface compared to that of a rectangular surface.

much faster at the edges than at the planar faces of the substrates, which will further increase the stresses along the edges of the substrate.[25] Finally, the stresses generated at the edges in the alumina films are further amplified at sharp edges of the substrates because the edges and notches act as "stress amplifiers".[23] We believe that the geometric and electric field factors contribute to the formation of the cracks in the aluminum films.

When the stress generated at these edges of the alumina films exceeds the fracture toughness of nanoporous alumina, the cracks in the films were observed.[23] The cracks followed the direction of highest stress along the edges of the substrate. The cracks in alumina films released the stress in the film, and the alumina films on the faces then continued to grow after crack formation.

For cylindrical substrates, the electric field distribution at its surface is much smoother (Figure 2C) than that of square aluminum substrates (Figure 2B). The uniform electric field suggests a uniform growth rate of the alumina film on the cylindrical substrates. The stress generated during alumina growth is distributed uniformly on the whole surface of the film. Thus, the absence of the cracks in the alumina films grown on cylindrical substrates is believed to be due to uniform alumina growth and lack of sharp edges on the cylindrical substrates. We also noticed the presence of a few low-electric-field intensity peaks (~5−10% of the average electric field intensity (~85 kV/m)) at the surface of the alumina in our calculations. These relatively smaller electric field intensity peaks are observed because of the limited calculation capabilities (low resolution) of our software. We expect the electric field intensity at the cylindrical substrates to be more uniform than is reported here. More intensive electric field calculations are underway in our group using the more powerful COMSOL Multiphysics software.

We have also estimated the amount of stresses in the flat alumina films by assuming that the stress is solely due to volume expansion during conversion of Al to Al_2O_3. In Griffin's theory,[23] the critical stress (σ_c) for crack propagation is given by $\sigma_c = (2E_{\text{nanoporous}}\gamma_s/\pi a)^{1/2}$ where $E_{\text{nanoporous}} = 253$ GPa[22] is the Young's modulus of nanoporous alumina, a is half of the crack length, γ_s is the specific surface energy of alumina; (γ_s ~2 N/m, see W. Pompe and H. J. Weiss in Current Topics in Material Science; Kaldis, E., Ed.; Northern−Holland, Amsterdam, 1985; Vol. 12, p 231). We have observed cracks at edges for ~1.5 μm thick films on rectangular substrates, i.e., $a = 750$ nm. Inserting these values in the above equation, we estimated $\sigma_c \approx 0.65$ GPa, which is in agreement with previously observed stress in the alumina films grown on aluminum.[21] The critical stress value is probably larger than the estimated value of ~0.65 GPa because of difficulties in knowing the exact film thickness at which cracks were formed in the film. It is possible that the cracks in the films occurred at film thickness less than 1.5 μm, which would indicate a higher critical stress value than the predicted value of 0.65 GPa.

Because $E_{\text{nanoporous}}$ and γ_s are constant for a given anodic alumina film, the crack length at which a crack initiates

(25) Bradhurst, D. H.; Leach, J. S. L. *J. Electrochem. Soc.* **1996**, *113*, 1245.

depend on σ_c and a. Given all other parameters (such as anodization voltage and time, size of aluminum, temperature, and concentration of electrolyte) remains constant, σ_c would largely depend on the degree of stress dissipation during anodization. If the stress generated during volume expansion can be dissipated such that the stress in the film does not exceed σ_c, then cracks in the film will not appear. Thus, it appears that the geometries of the aluminum substrates may have a significant effect on the crack formation and propagation. For example, it is shown in this work that the cracks were not observed in the alumina films grown on the planar aluminum sheets and on the cylindrical aluminum rods. The cracks, however, were observed in alumina films at the edges of square and rectangular substrates because of amplified stresses at these edges and the inability of the film to relieve these stresses because of constrained boundaries at these edges. Similar results were observed for triangular and hexagonal substrates, where cracks were developed at sharp edges of the substrates (data not shown).

IIIB. Merging and Curving of Nanopores in Cylindrical Substrates. Due to sanding of the substrates with 400, 600, and 1500 grit sandpapers, the substrates had some beveled planes on them even after electropolishing of the substrates (Figure 3A). A closer look at the nanoporous film revealed some very interesting information about the growth of the alumina nanopores grown on substrates with beveled planes. First, the cross-section of alumina films indicates that the nanopores always initiate perpendicular to beveled planes (Figure 3A). This is denoted by dashed arrows at various places on the electron micrographs. Second, some of the pores grown on two beveled planes merged with their adjacent pores (denoted by dotted circles in Figure 3A). Silica nanotubes synthesized in the pores have also confirmed the pore merging (Figure 3C, vide infra). Third, some of the pores appeared to curve before they merged with their adjacent pores (dotted arrows in Figure 3A). Finally, unlike alumina films grown on rectangular and square substrates, no cracks were observed in the films grown on cylindrical substrates (see above). We now propose a model to explain the nanopore merging in the alumina films grown on aluminum substrates with beveled planes and comment on possible reasons of curving of pores prior to their merging.

IIIC. Proposed Model for Merging and Curving of the Nanopores on Beveled Planes on Cylindrical Substrates. The exact mechanism of the self-order and highly organized cylindrical pore formation in alumina is still debated.[14] The equilibrium between electric-field-assisted oxide dissolution at the oxide/electrolyte interface and oxide formation at the metal/oxide interface is supposed to result in the growth of alumina porous membranes.[14] The oxidation of aluminum to alumina results in considerable stresses, and the mechanical stress at the Al/Al_2O_3 interface is proposed to cause repulsion forces, which promote self-organized and ordered cylindrical nanopores in anodic alumina.[14a] There is, however, no mechanism reported in the literature that explains the curving and merging of nanopores in the alumina films.

IIID. Pore Growth and Pore Merging Mechanism in Alumina Films on Cylindrical Substrates. Figure 4A schematically shows the proposed model for the growth of nanopores on the beveled faces of a cylindrical aluminum substrate. There are three important steps in the formation of merged pores grown on beveled planes: nucleation, pore

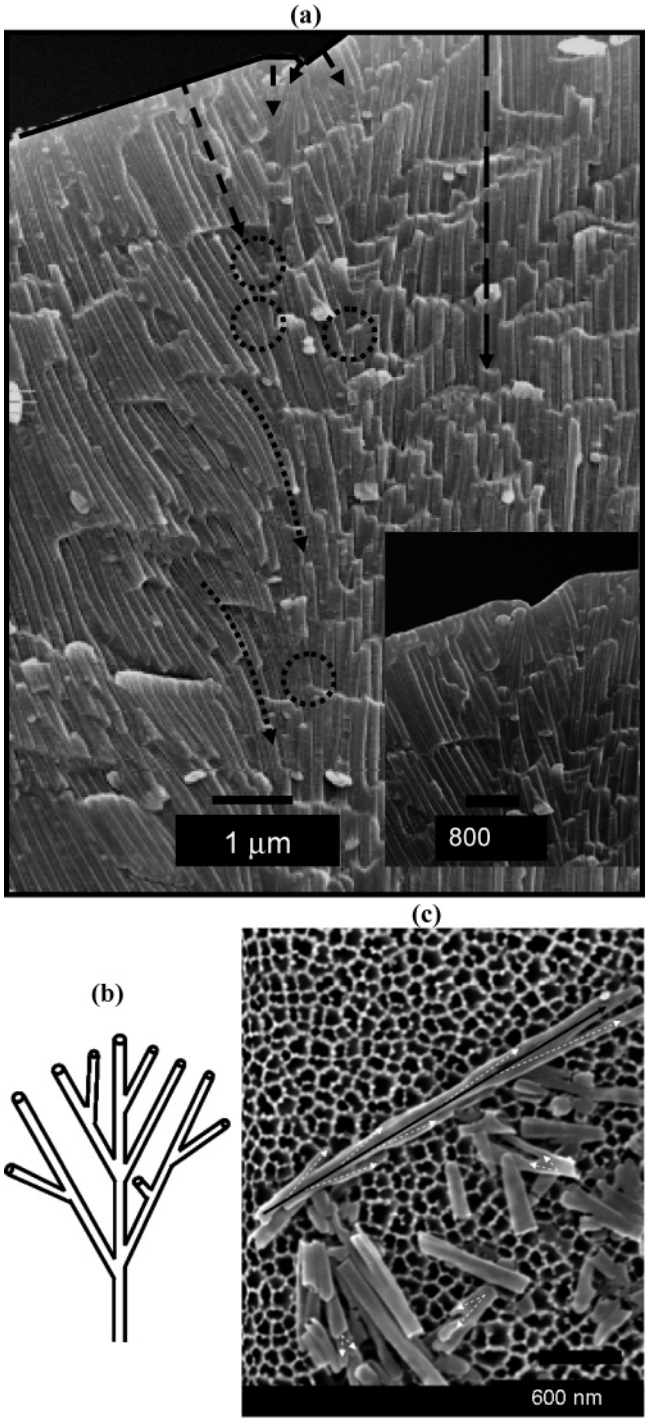

Figure 3. (A) Scanning electron micrograph (SEM) of a cross-section of alumina nanoporous film grown on beveled faces. The pores always nucleated perpendicular to the surface, as denoted by dashed arrows. The dotted circles show pore merging. whereas dotted arrows represent curving of the pores. $\vec{E}_{highest}$ denotes the direction of highest electric field strength. Inset image shows a higher-magnification SEM of the top-right portion. (B) Schematic presentation of the dendritic pores grown on a cylindrical aluminum substrate with beveled planes. (C) Typical SEM of the dendritic silica nanotubes synthesized in alumina films grown on cylindrical aluminum rods. The dendritic structures clearly showed the merging of pores (dotted white arrows) with a "dominant" pore (denoted by black solid arrow) and confirmed that the pores were open at the pore merging intersection−junction. The presence of multiple broken segments indicates that the silica nanotubes were mechanically fragile.

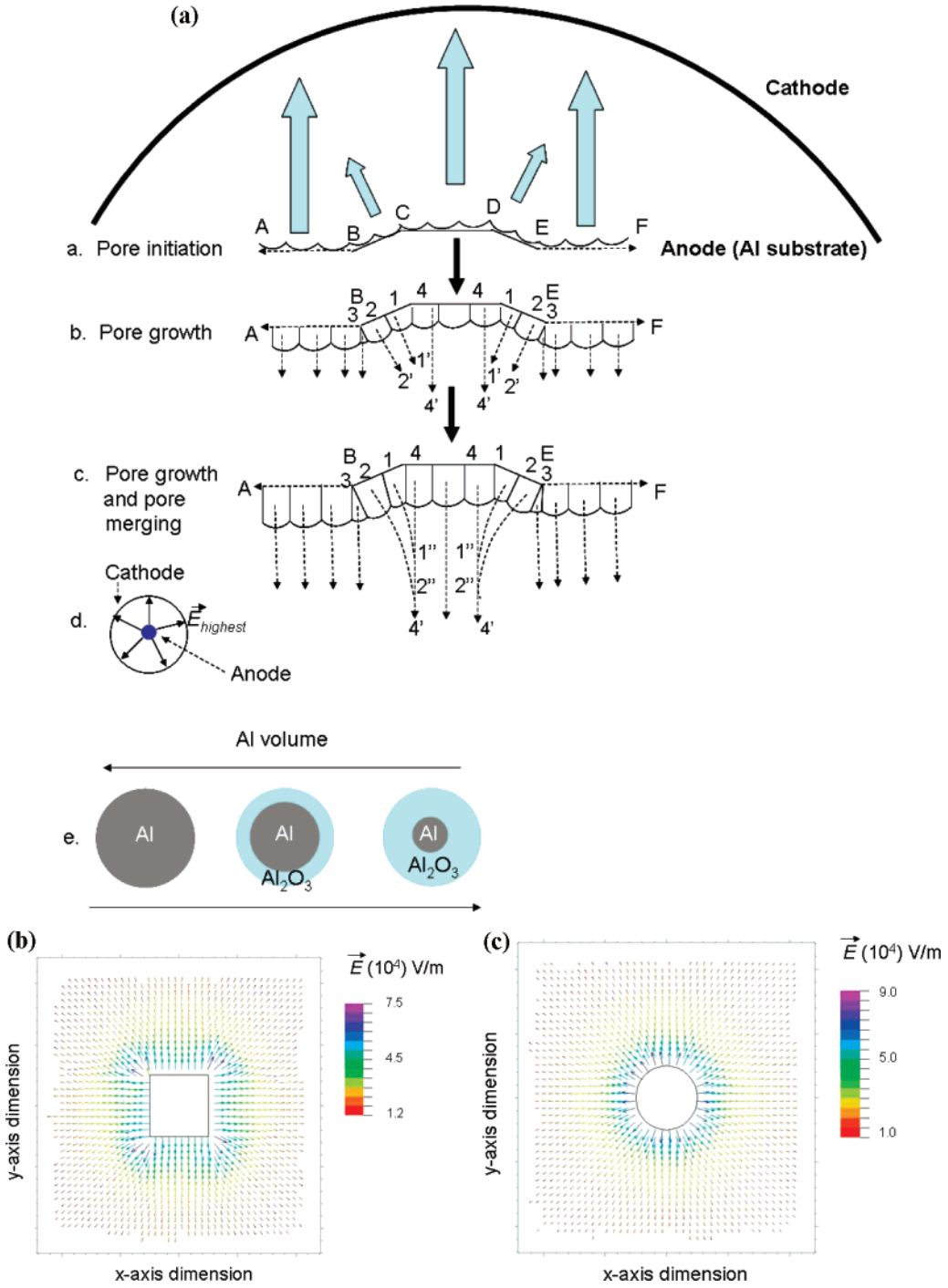

Figure 4. (A) Proposed mechanism of pore merging and curving. The cathode and anode are not drawn to scale. Compared to the cathode, the anode is drawn larger than its actual dimension. The cathode diameter to anode diameter ratio was ~20. The arrows depict the direction of the electric field sensed by pores nucleated at the surface. (a) Pore initiation on the aluminum substrate; (b) pore growth; (c) pore growth and pore merging (pore curving is also shown before pore merging); (d) arrows show the direction of $\vec{E}_{highest}$ sensed by the anode (inner dashed circle). Note that $\vec{E}_{highest}$ is along a line joining the center of the blue circle (anode) to a larger circle (cathode). (e) Volume fraction of aluminum decreased with alumina growth, whereas alumina fraction increased with growth time. The direction of the electric field at the surface of a square and a cylindrical substrate are shown in B and C. The color code for these figures is same as that described in parts B and C of Figure 2.

growth, and pore merging. According to this model, the pore size and density and its orientation in the anodically oxidized aluminum depend on the spatial, electric field, energetic, and kinetics factors. We now discuss various factors that affect the direction, growth rate, and orientation of nanopores in the alumina film grown on cylindrical substrates.

1. Effect of Electric Field and Energetics on the Pore Nucleation. We first note that the electric field is the driving force for the pore growth in the alumina films, and the direction of the electric field will significantly influence the nanopore growth direction. Because the ratio of the diameter of cathode to that of the anode (aluminum) is very large in our experimental setup, the electric field observed by the anode is approximately perpendicular to its respective surface (panels B and C of Figure 4). This results in the nucleation of pores perpendicular to their surfaces (Figures 3A, 5, and 6).

The formation of nanoporous alumina involves the migration of Al^{3+} (formed at the metal/metal-oxide interface) and O^{2-} (generated at the metal-oxide/solution interface) ions under applied external voltage for the formation of Al_2O_3. The anodic alumina growth on a flat substrate produces straight cylindrical nanopores because the resistance to the migration of ions (Al^{3+}, O^{2-}, and OH^-) is minimum for cylindrical pores that grow along the highest electric field direction (i.e., perpendicular to the surface of the anode). On the other hand, the pores that do not grow perpendicular to the anode surface would experience a larger ionic resistance because the ions would migrate a longer distance than those ions present in pores growing perpendicular to the surface, and these pores will not sustain uniform growth. Accordingly in our case, the pores always nucleated perpendicular to the anode surface.

2. Effect of Spatial Factors on Pore Merging. We propose that spatial factors strongly affect the orientation of pore growth and pore merging in the alumina film following pore nucleation. For a cylindrical substrate, the spatial volume available for nanopores (1, 2, and 4) to uniformly grow in 11′, 22′ and 44′ directions decreases with alumina growth (Figure 4A, part e). This is because the surface area of an aluminum cylindrical rod decreases with alumina growth. To compensate for reduced spatial volume available for alumina growth, we propose that there must be a restructuring nanopore growth mechanism such that some pores grow with anodization process, whereas others either cease to grow (termination of the pores) or merge with adjacent pores. We did not observe termination of the pores, but our experimental data indicated that some pores merged (called "merged" pores) with their adjacent pores (called "dominant" pores). The diameter of the merged pores (depicted as dashed white arrows in Figure 3C) is about 30−70% smaller than the diameter of the dominant pore (black solid line in Figure 3C). This observation also suggests that the local electric field strength sensed by merged pores is smaller than the electric field sensed by dominant pores. This is probably because the growth direction of the merging pores is not along the highest-electric-field direction, whereas the dominant pores grew along the highest-electric-field direction. These observations are consistent with a recent report by Chen and co-workers.[16b] They observed that insufficient spatial volume for uniform growth of two pores resulted in the merging of the pores and that the dominant pore takes over its adjacent pore. They also attributed this phenomenon to steric and electric-field effects.

It should also be noted that we did not observe cracks in the alumina films grown on the beveled planes of cylindrical substrates even though these substrates have sharp edges. This is because a crack does not develop until the length of a crack reaches a critical value (*a* in the Griffin's equation, see above). For the beveled cylindrical substrates, the critical crack length was not attained in our experiments; the cracks thus did not develop in these films.

3. Kinetic Effects. From the kinetics view point, for pores 1 and 2 to continuously grow along 11′ and 22′ directions, pores 1 and 2 must grow faster than pore 4 to compensate for their slanted growth direction (Figure 4A). This is, of course, kinetically unfavorable because the growth rate of pores originating at different planar faces do not change significantly under our experimental conditions. Indeed, we have experimentally observed that the length of the nanopores measured between the air/alumina interface and points at which the pores start propagating to grow parallel to one another is the same (within ±5%, Figure 5). The length of pores was determined by drawing lines along the pores and estimated using Adobe Acrobat (version 5.0) software. The slight differences in the calculated length of the different pores were probably due to errors involved in drawing lines along the pores using the employed technique.

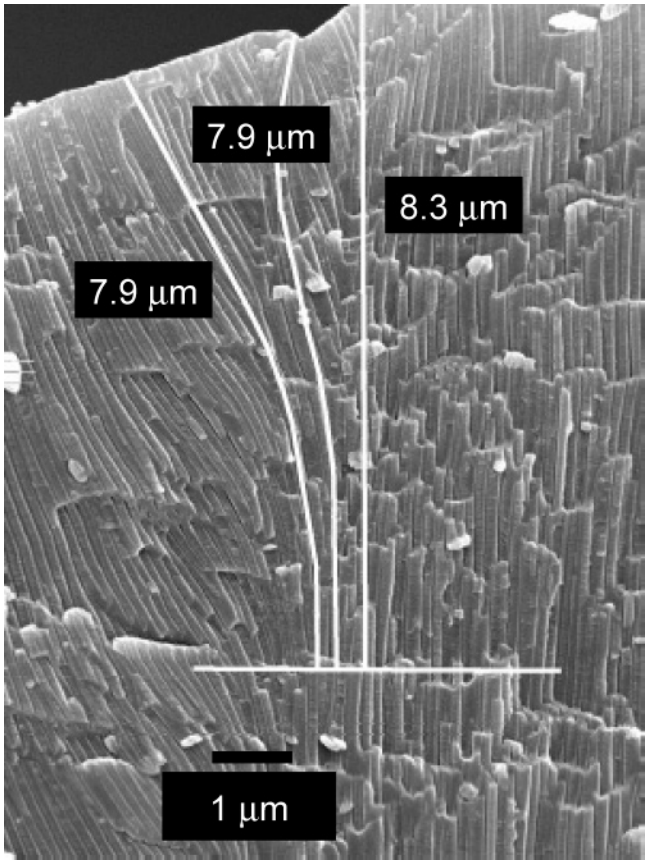

Figure 5. Estimated length of nanopores between the air/alumina interface and a point where the pores grew parallel to each other. The estimated lengths of three different pores were within 5% of each other.

From the above discussion, we believe that the combined effects of steric, kinetics, energetic, and the strength and direction of the electric field contribute to the orientation, growth rate, and merging of alumina nanopores grown on beveled faces of the cylindrical aluminum substrates.

IIIE. Curving of Nanopores (Figure 3A). The curving of nanopores in anodic aluminum oxide films has been previously observed, but its explanation was not given in those reports.[17] One plausible reason of this curving is that near the intersection of pores, the direction of the electric field slightly changes because of a self-adjusting electric field to sustain nanopore growth along the highest-electric-field direction. For example, pores 1 and 4 grow in the 11′ and 44′ directions, respectively (Figure 4). During its growth and near its point of intersection with pore 4, pore 1 feels two different electric field forces along the 11′ and 44′ directions.

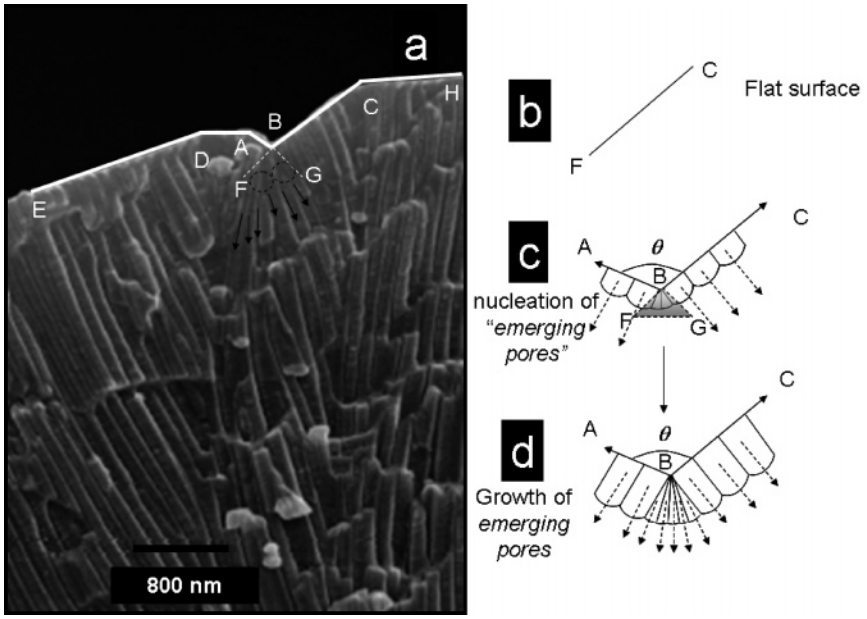

Figure 6. Schematic of pore emerging mechanism: (a) SEM of a cross-section of alumina where the pore density was significantly higher than the rest of the film. EDABCH is the top substrate surface where the pores were initiated. Black arrows show six nanopores emerged at point B. (b) Cartoon representing a flat planar substrate. (c) Nucleation of emerging pores from two beveled AB and BC planes after splitting of pores into two or more pores. θ is the angle between AB and BC planes. (d) Growth of the "emerging pores".

Table 2. Relationship between θ and Pore Orientation and Density

angle between beveled planes (θ)	pore orientation/density
180	pores grow parallel to each other
<180	pore density is higher than that of flat surface
>180	pore merging is observed

The result of these two electric-field forces is believed to contribute to curving of the pores prior to their merging.

IIIF. Increased Density of Initiated Nanopores on Beveled Faces (Emergence of New Pores). The pore density in alumina films depends on the surface roughness, the number of faces (such as shown in Figure 6), and the angle (θ) between two faces. Higher surface roughness and number of faces available on the substrate will produce a higher number of the nanopores in the anodic alumina because of increased surface area on which the nanopores can initiate and grow.

Interestingly, we have observed an unexpectedly large number of pores close to point B (Figure 6a). For example, the number of pores emerged per unit area close to point B was almost six times higher (denoted by black arrows) than the number of pores present in the DE segment (Figure 6a). Because of the geometrical discontinuity at point B, all the pores nucleate at or close to point B and within the BFG volume were approximately perpendicular to point B (i.e., along the highest-electric-field direction). Compared to flat planar substrates (Figure 6b or ED in Figure 6a), the beveled faces such as BFG have excess space (Figure 6c) that must contain pores. There are at least two possibilities for filling of BFG: (1) a larger number of pores, i.e., pore emerging; and (2) larger pores. Larger pores are defined as the pores whose pore diameter is larger than the pores originating from the flat surfaces under the same experimental conditions, whereas the larger number of pores is defined as the formation of more pores than are expected for the flat surfaces. We did not observe larger pores in the BFG area. In fact, the pore size at the nucleation site (point B in Figure 6a) is much smaller than the size of pores nucleating at flat faces (such as ED in Figure 6a). On the other hand, we found that the BFG area contains a significantly larger number of nanopores after splitting of pores into two or more pores (dotted circle in Figure 6a). We attribute the emergence of unexpectedly large number of pores to the availability of excess BFG space.

Table 2 shows the dependence of the orientation and pore density on θ. For example, when $\theta = 180°$ (i.e., flat aluminum substrates) our model predicts the pores will be parallel to one another and perpendicular to the surface (Figure 1) because the electric field observed by the anode is perpendicular to its surface. When $\theta < 180°$, the nanopore density will be higher than that of a flat surface (Figure 6) because of excess volume available for pore formation. Finally, for $\theta > 180°$, the merging of nanotubes with adjacent nanotubes occurs (Figure 3). For a special case when $\theta = 270°$, our model predicts that the pores on adjacent faces will grow perpendicular to each other and also to their respective surfaces. This is, indeed, experimentally observed. The nanopores on a substrate with $\theta = 270°$ grew perpendicular on two faces (see the Supporting Information, Figure 2S).

IIIG. Dendritic Nanopore Formation. The proposed model also predicts that the alumina nanopores grown on beveled faces of cylindrical substrates would produce Y-shaped and dendritic nanopores because of merging of pores with their adjacent pores. To prove that the nanopores grown on cylindrical substrates are dendritic, we performed template synthesis of silica nanotubes using sol−gel chemistry in the alumina films synthesized on cylindrical substrates. The

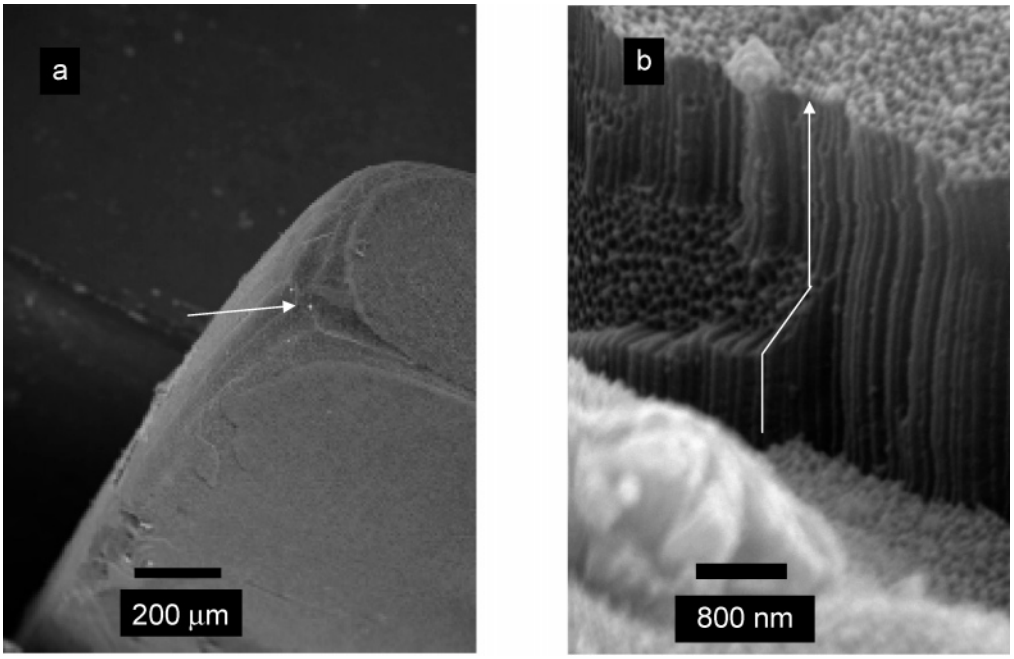

Figure 7. (A) Low-magnification SEM of alumina film grown on a rectangular aluminum rod where 90° bends were observed. (B) High-magnification SEM showing two 90° bends in the alumina film.

detail of the silica deposition procedure is described in the Materials and Methods section. SEMs in Figures 3C and 6S clearly show dendritic silica nanotubes with branching along their length. The wall thickness of the nanotubes is between ~3−6 nm, and the nanotubes are mechanically very fragile (see the Supporting Information, Figure 3S). Even after our repeated careful sample preparations, many of our silica nanotubes were broken because of their fragile nature. This can be seen in Figure 3C, where many broken but branched silica nanotubes are present in the electron micrograph. The branching of silica nanotubes also proved that the merging nanopores were opened at the interjunctions of the merging nanotubes so that silica can be deposited at these junctions.

We have not quantitatively investigated in detail the factors that affect the degree of branching in these films. We expect that the degree of pore branching in the alumina films grown on the cylindrical rods would increase with an increase in the alumina film thickness and pore diameter and that it would decrease with an increase in the aluminum rod diameter. Clearly, a more detailed study is needed to investigate the dependence of the alumina pore density on different substrate geometry and alumina growth parameters.

The nanoporous films synthesized in this study have many characteristics that differentiate them from commercially available nanoporous alumina membranes (from Whatman). For example, Whatman nanoporous alumina membranes commonly labeled as "20 nm pore diameter" have pore diameters of (200 ± 100) nm that span the whole thickness of the membrane except for the top 100−200 nm, where the pore diameter is ~20 nm. Thus, the branching of the nanopores from ~200 to ~ 20 nm occurs in the top ~200 nm of the membranes. In contrast, the branching of the nanopores in our films occurs throughout the whole thickness of the films, and the degree of branching in the nanoporous alumina can be controlled through different material and process parameters.

Finally, we have also observed extremely interesting pores that appear to contain 90° bends in them (Figure 7B). We found these nanopores at the intersection of three planes of rectangular substrates (Figure 7A). At present, the exact cause of the formation of 90° bent-stepped nanopores is not clearly understood. One plausible explanation is that these nanostructures are formed because of complex electric field and internal strain effects present at the intersection of three planes. A more detailed investigation on the mechanism of the formation of these interesting nanoporous structures will be published in the near future.

Why did nonlinear pores not attract the attention of researchers in the past? Historically, alumina and polymer nanopore membranes are studied on flat surfaces and have been primarily used as filters for many decades (such as commercially available alumina filters from Whatman International). In the 1990s, the alumina and polymer nano- and microporous filters have attracted a lot of attention for their use as templates for the synthesis of nanomaterials.[1] Because linear nanopores containing alumina and polymeric templates are easier to synthesize than nonlinear nanopores templates, most of the studies to date have involved the use of linear nanopores and nanotubes. Recently, nonlinear nanopores and nanotubes have gained much attention and a few reports have emerged describing their synthesis, characterization, and applications in basic and applied sciences.[3,16c−16f,24] The controlled synthesis of complex-shaped nanotubes and nanowires is crucial to further advancing their applications in the fields of nanoelectronics, biosensing, bioseparations, catalysis, etc. The fabrication of complex nanocircuitry is hampered by difficulties in the synthesis and manipulation of complex-shaped nanotubes and nanowires at the nanoscale level. Using nonlinear nanopores containing alumina films similar to those reported in this paper as templates, one can reproducibly and inexpensively synthesize nanotubes and nanowires of complex shapes in large quantities that may

otherwise be difficult to prepare using other conventional methods (such as electron- and photolithographies). This would open new possibilities for nanodevice (such as nanoelectronic and nanofluidic) fabrications.[26,27] Other potential applications of these nanoporous films are in the fields of biosensing, bioseparations, and catalysis. From a fundamental viewpoint, nonlinear nanopores and nanotubes may exhibit interesting optical, electrical, and magnetic properties.

IV. Summary

Nonlinear nanopores of complex shapes (such as dendritic and curved pores) are synthesized by the anodic oxidation of different geometric aluminum substrates. It is found that the curving of the alumina pores occurs prior to their merging with their adjacent pores. A qualitative mechanism is proposed that predicts the orientation, curving, merging, and pore density of nanopores on the basis of spatial, energetic, electric field, and kinetics factors. These films are expected to find applications in fields such as nanodevice fabrications, biosensing, bioseparations, nano-optics, and catalysis, where complex shapes of nanotubes and nanowires may be needed.

Acknowledgment. We acknowledge the National Science Foundation (Grant 0609349), ORDA, and MTC (SIUC) for funding of this project. We also acknowledge Prof. Luke Tolley for use of his machining facility and for interesting discussions. We thank Drs. Steve Schmitt and John Bozzola of the IMAGE center at SIUC for helping with SEM and TEM analysis, and Mrs. Bita Zakeri for helping with graphics.

Supporting Information Available: Figures 1S−6S. This material is available free of charge via the Internet at http://pubs.acs.org.

CM062595O

(26) Xiang, J.; Lu, W.; Hu, Y.; Wu, Y.; Hao, Y.; Lieber, C. M. *Nature* **2006**, *441,* 489−493.

(27) Huang, Y.; Duan, X.; Lieber, C. M. Semiconductor Nanowires: Nanoscale Electronics and Opto-electronics. In *Dekker Encyclopedia of Nanoscience and Nanotechnology*; Schwartz, J. A., Ed.; Marcel Dekker: New York, 2005.